Electronic Supplementary Information (ESI)

Thermoelectrochemical Formation of Fe/Fe_3C@Hollow N-Doped Carbon in Molten Salts for Enhanced Catalysis

Wei Weng,[ac] Jing Zhou,[b] Dong Gu[b] and Wei Xiao[a] *

a. College of Chemistry and Molecular Sciences, Hubei Key Laboratory of Electrochemical Power Sources, Wuhan University, Wuhan 430072 (P. R. China)
b. The Institute of Advanced Studies, Wuhan University, Wuhan 430072 (P. R. China)
c. School of Resource and Environmental Sciences, Hubei International Scientific and Technological Cooperation Base of Sustainable Resource and Energy, Wuhan University, Wuhan 430072 (P. R. China)

* Email: 00030042@whu.edu.cn Homepage: http://wxiao.whu.edu.cn/

Experimental Details

Materials: NaCl (anhydrous, 99% purity) and $CaCl_2$ (anhydrous, 99% purity) were purchased from Shanghai Titan Scientific Co. Ltd. Tris (hydroxymethyl) aminomethane (Tris, >99.99%) was obtained from the Shanghai Regal Biology Technology Co. Ltd. Dopamine hydrochloride (>99%) was provided by the Hefei Bomei Biotechnology. Co. Ltd. $FeCl_3$ (Analytical reagent, 99.9% in purity) was purchased from the Aladdin (Shanghai, China). H_2O_2 (30 wt%) was purchased from Sinopharm Chemical Reagent Co., Ltd. Sodium phosphate monobasic (NaH_2PO_4, >99.0 %), commercial Pt/C (20 wt% Pt), and 5 wt% Nafion solution were purchased from Sigma-Aldrich.

Preparation of Fe_2O_3@PDA: The preparation of Fe_2O_3 was carried out according to a previous report.[1] 2.7 g $FeCl_3$ was dissolved in 500 mL of deionized (DI) water, followed by adding 27 mg NaH_2PO_4. After stirring for 1 h, the mixture was sealed in a Teflon-lined stainless-steel autoclave, followed by heating at 105 ^oC for 48 h. Then, Fe_2O_3 nanospindles (Fig. S1a and c) were obtained after centrifugation in DI water and ethanol for several times and vacuum-drying at 60 ^oC overnight. 200 mg Fe_2O_3 nanospindles were added into 200 mL (10 mM) Tris buffer solution, followed by addition of 200 mg dopamine hydrochloride. After stirring for 20 h at room temperature, the Fe_2O_3@PDA powders (Fig. S1b and d) were collected by centrifugation in DI water and ethanol for several times and vacuum-drying at 60 ^oC for overnight.[2, 3]

Reaction mechanism investigation: Pyrolysis of Fe_2O_3@PDA in the inert Argon atmosphere is conducted at 600 ^oC for 2 h (denoted as 0 V, 2 h in air). For comparison, pyrolysis of Fe_2O_3@PDA is also conducted in the NaCl-$CaCl_2$ molten salt at 600 ^oC for 2 h (denoted as 0 V, 2 h in molten salt). To better understand the reaction mechanism, the above-mentioned pyrolysis products were only leached in DI water for 12 h to remain all iron intermediates, followed by vacuum-drying at 60 ^oC overnight. Similarly, products obtained by electrochemical treatment of Fe_2O_3@PDA in the NaCl-$CaCl_2$ molten salt at 2.1 V for 2 h are also leached in DI water for 12 h to remain all iron

species in some cases, followed by vacuum-drying at 60 °C overnight (denoted as 2.1 V, 2 h in molten salt). The gaseous products during the pyrolysis of Fe_2O_3@PDA in Ar atmosphere were analyzed by a gas chromatograph (GC-2014C plus, Shimadzu, Japan) equipped with a thermal conductivity detector (TCD), two flame ionization detectors (FID-1 and FID-2) and a chromatographic column (Rtx-1).

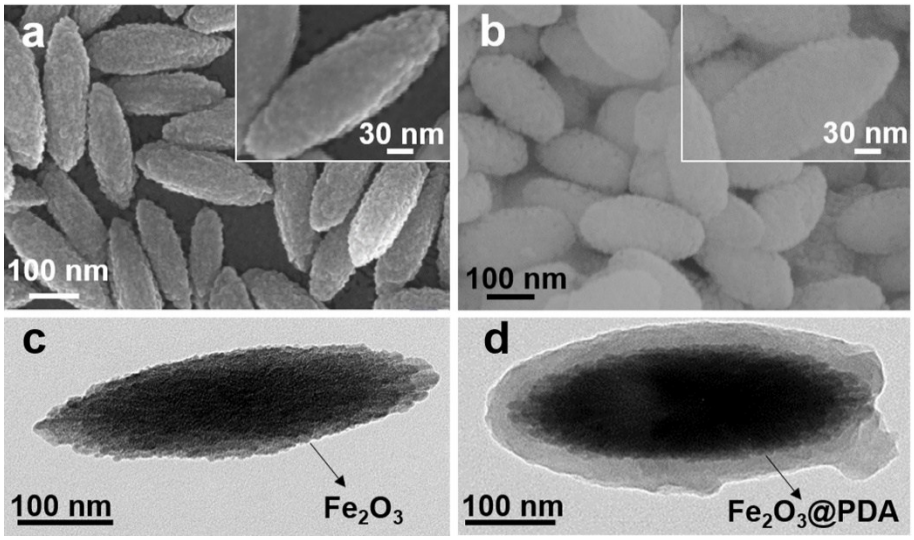

Fig. S1 SEM (a,b) and TEM (c,d) images for Fe_2O_3 (a,c) and Fe_2O_3@PDA (b,d).

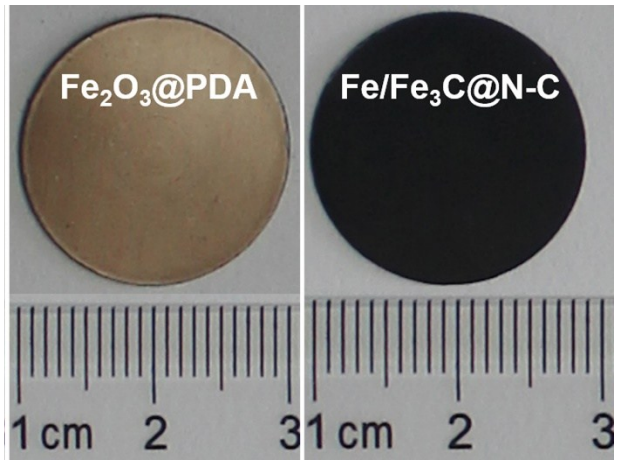

Fig. S2 Optical images of the Fe_2O_3@PDA pellet before electrolysis (left) and the obtained Fe/Fe_3C@N-C pellets after electrolysis (right).

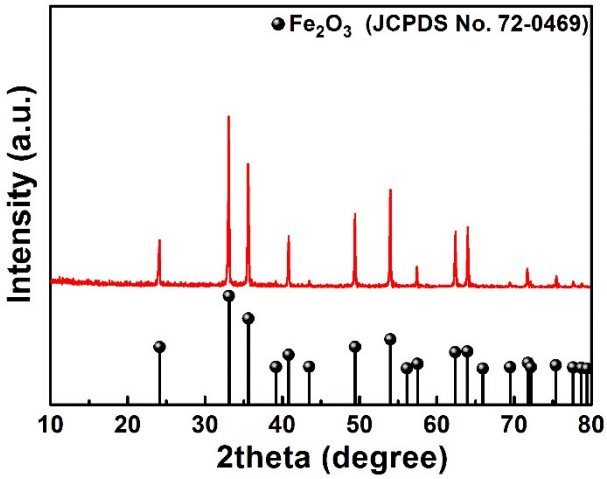

Fig. S3 XRD pattern of the Fe_2O_3@PDA.

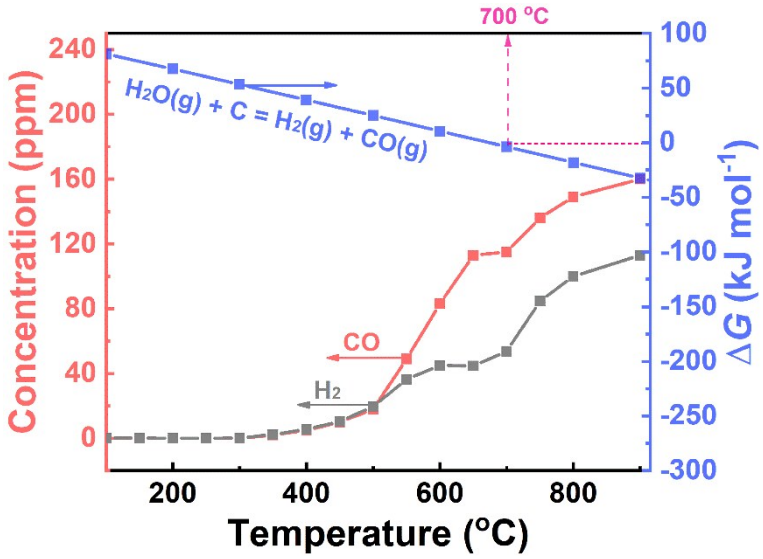

Fig. S4 Concentration variations of H_2 and CO during the pyrolysis process of PDA in Ar atmosphere (5 ^{o}C min^{-1}) as well as the Gibbs free energy changes (calculated by HSC 6.1) of reaction H_2O (g) + C = H_2 (g) + CO (g).

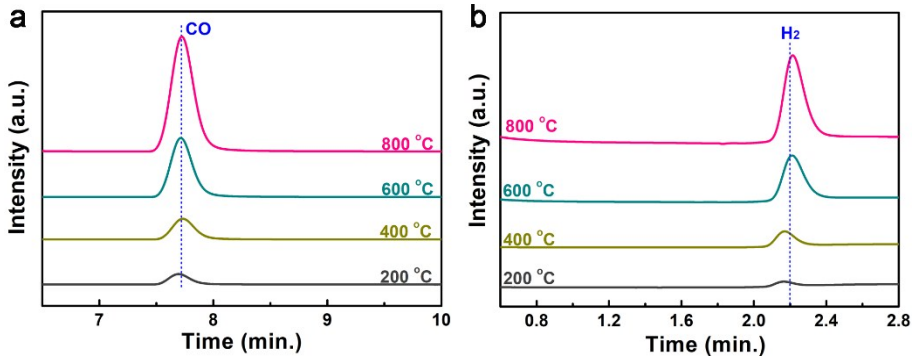

Fig. S5 GC spectra of the outlet gas during the pyrolysis process of PDA in Ar atmosphere: (a) CO; (b) H_2. Both the H_2 and CO are detected by a thermal conductivity detector (TCD).

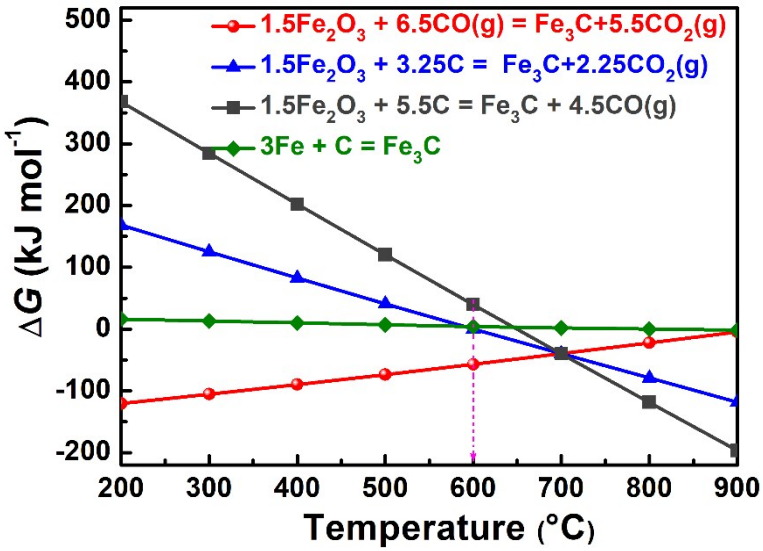

Fig. S6 Gibbs free energy changes of possible reactions for Fe_3C formation (calculated by HSC 6.1 software).

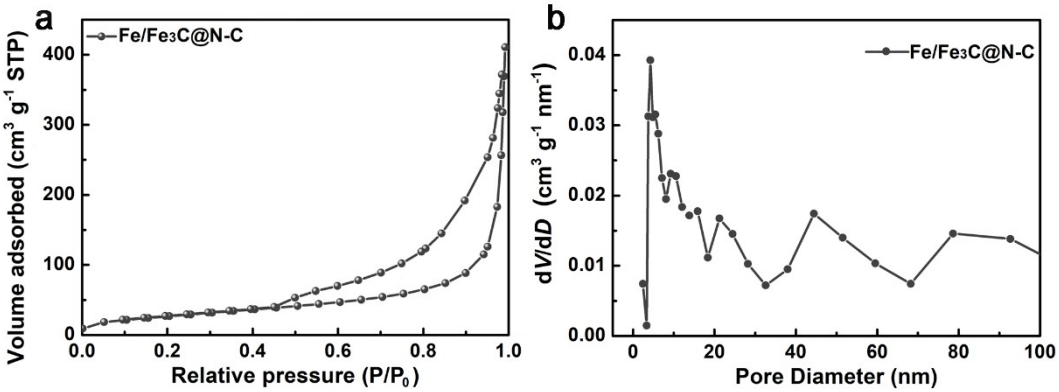

Fig. S7 Nitrogen adsorption-desorption isotherm (a) and pore size distribution (b).

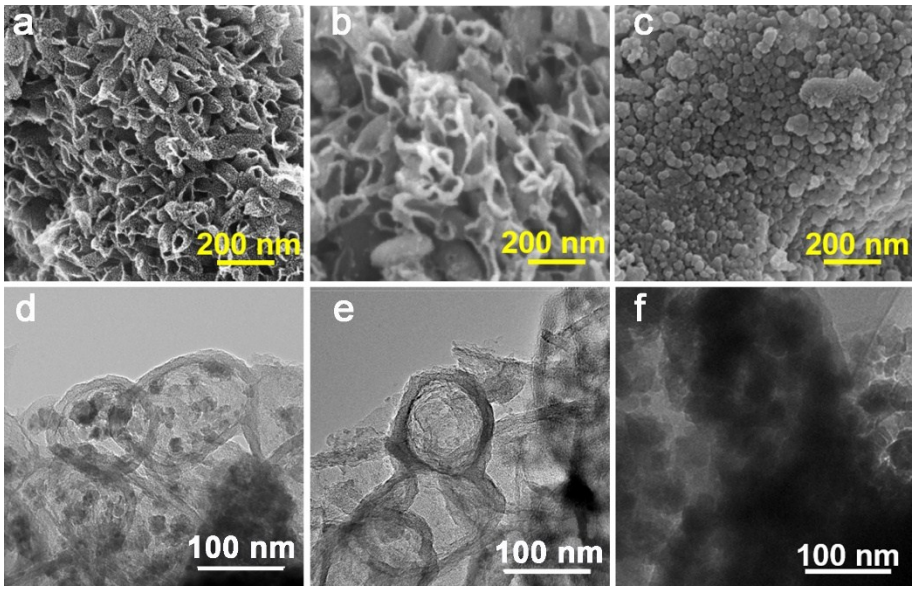

Fig. S8 SEM (a-c) and TEM (d-f) images for Fe/Fe_3C@N-C (a,d), N-C (b,e), and Fe/Fe_3C (c,f).

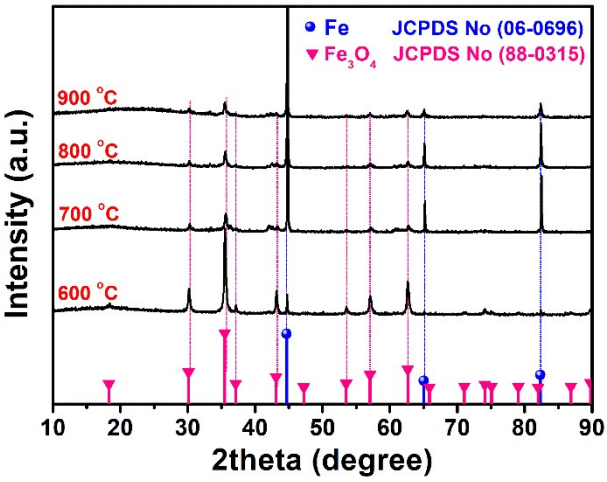

Fig. S9 XRD patterns for the pyrolysis product of Fe_2O_3@PDA in Ar atmosphere at different temperatures. Reaction time: 2 h. The obtained products were only leached in deionized water for 12 h to remain all iron intermediates, followed by vacuum-drying at 60 °C overnight.

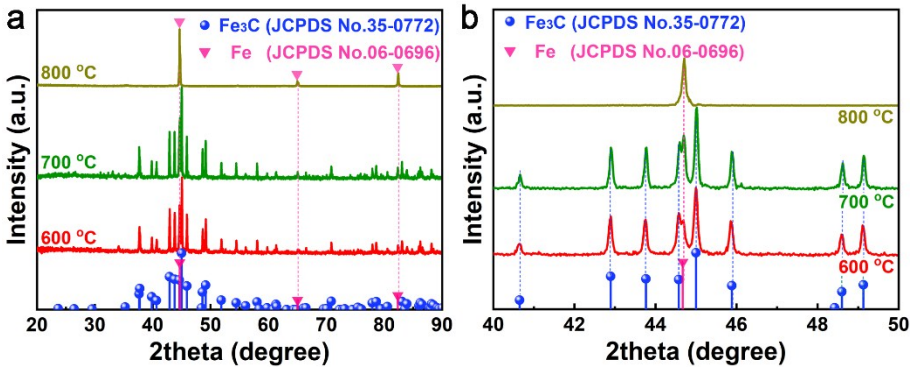

Fig. S10 XRD patterns of the products obtained by electrochemical treatments of Fe_2O_3@PDA in NaCl-$CaCl_2$ molten salt at 2.1 V for 2 h at different temperatures. The products were only leached in deionized water for 12 h to remain all iron species, followed by vacuum-drying at 60 °C overnight. The 2theta degree presented is in the range of 20-90° for (a) and 40-50° for (b).

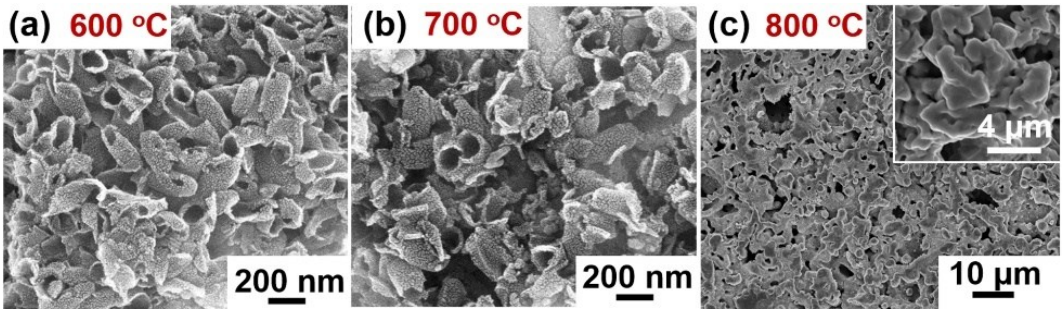

Fig. S11 SEM images for the products obtained at different temperatures from electrochemical treatment of Fe_2O_3@PDA pellets in NaCl-$CaCl_2$ molten salt at 2.1 V for 2 h. (a) 600 °C; (b) 700 °C; (c) 800 °C.

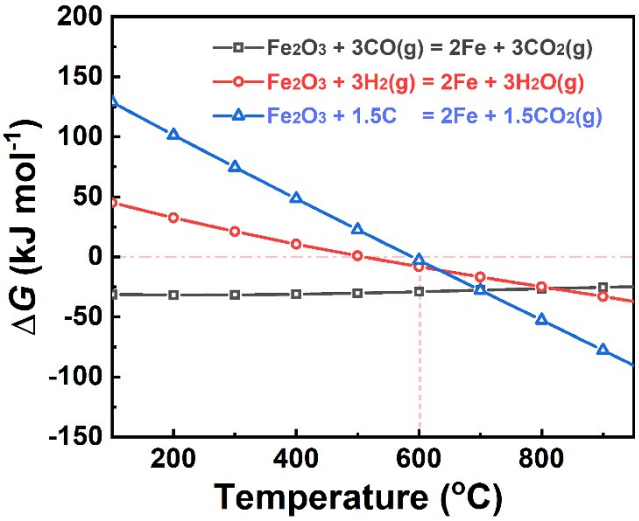

Fig. S12 Gibbs free energy changes (calculated by HSC 6.1 software) of related reactions for Fe formation.

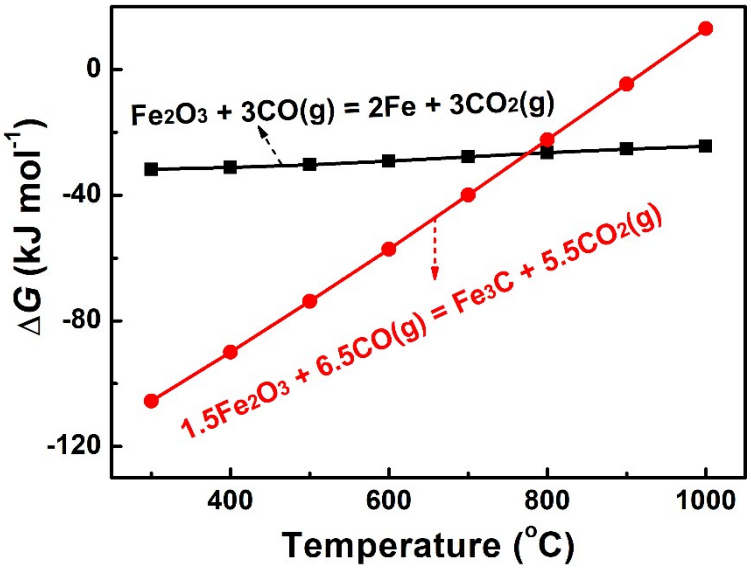

Fig. S13 Gibbs free energy changes (calculated by HSC 6.1 software) for reactions between CO and Fe_2O_3.

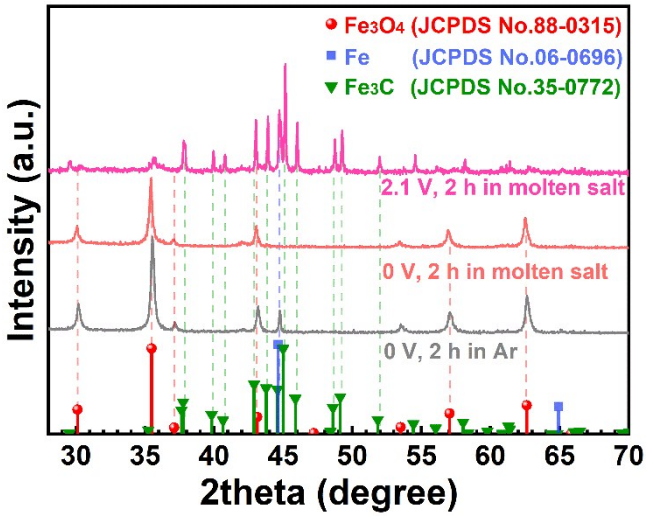

Fig. S14 XRD patterns of products obtained by treatment of Fe_2O_3@PDA at 600 °C in three different ways. Products were only leached in deionized water, without washing in acid solution. (0 V means that no voltage is exerted.)

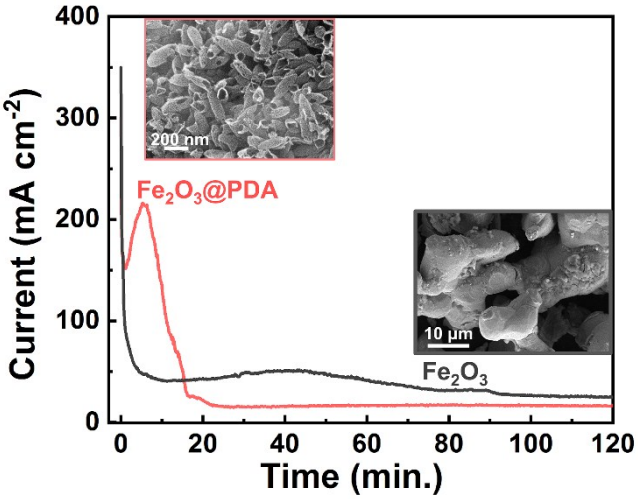

Fig. S15 Current-time curves for electrolysis of Fe_2O_3@PDA and Fe_2O_3 spindles. Insets are the SEM images of products obtained from the electrolysis of Fe_2O_3@PDA (left) and Fe_2O_3 (right) spindles. Electrolysis voltage: 2.1 V. Electrolysis time: 120 min.

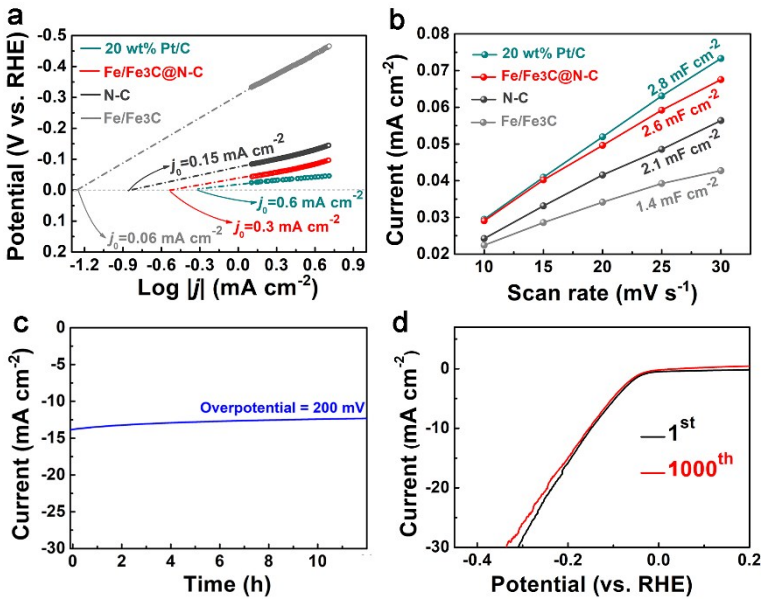

Fig. S16 HER performance of Fe/Fe_3C@N-C measured in 0.5 M H_2SO_4 solution: (a) calculation of exchange current density, (b) linear relationship between the capacitance current density and the scan rate, (c) long-term stability test performed under a constant overpotential of 200 mV, and (d) LSV curves of the first and 1000th repeated cycles at 10 mV s^{-1}.

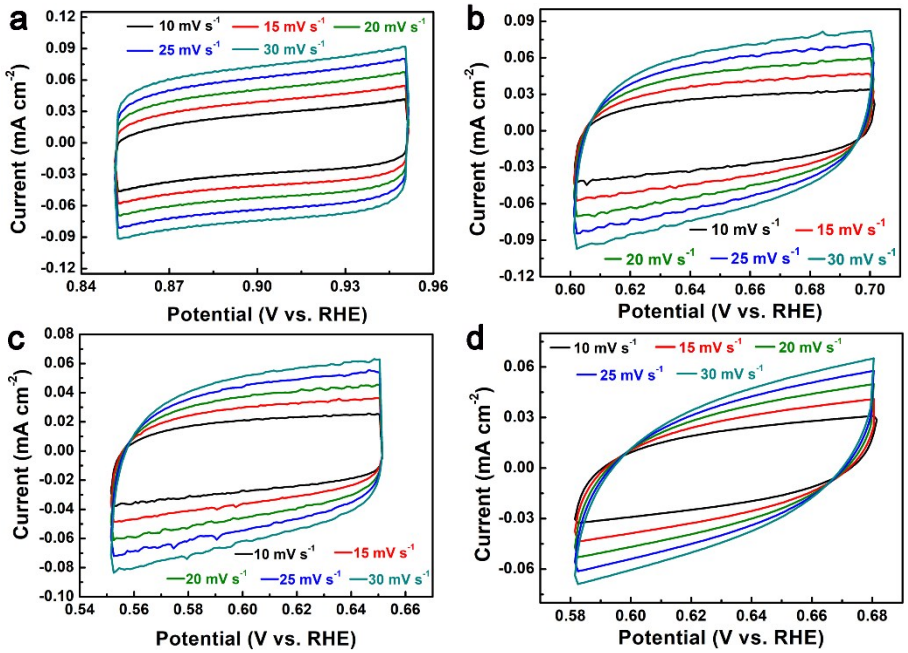

Fig. S17 CV curves of the 20 wt% Pt/C (a), Fe/Fe_3C@N-C (b), N-C (c), and Fe/Fe_3C (d) in non-Faraday regions at different scan rate in 0.5 M H_2SO_4 solution.

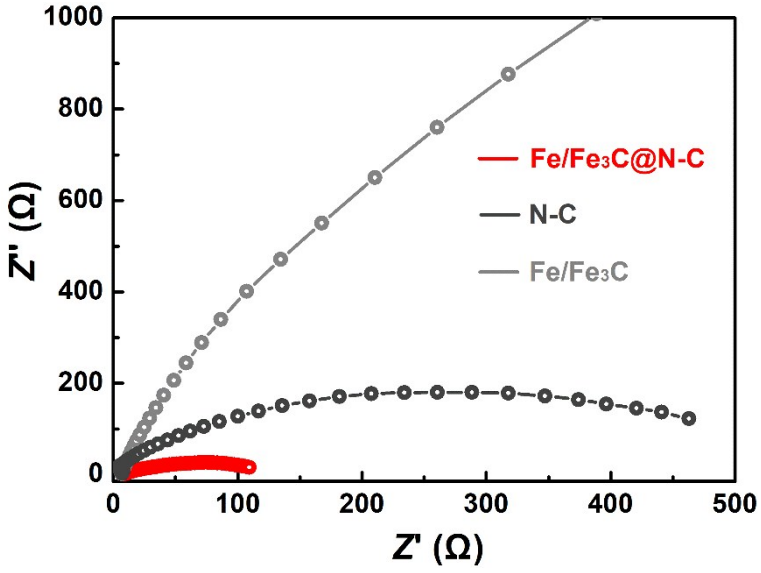

Fig. S18 Nyquist plots recorded at a HER overpotential of 150 mV in 0.5 M H_2SO_4.

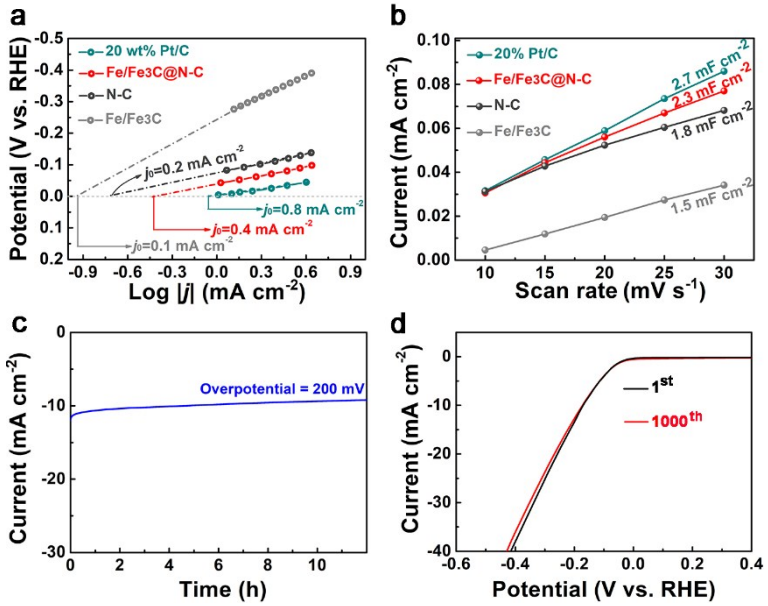

Fig. S19 Hydrogen evolution reaction performance of electrocatalysts measured in 1 M KOH solution: (a) calculation of exchange current density, (b) linear relationship between the capacitance current density and the scan rate, (c) long-term stability test performed under constant overpotential of 200 mV, and (d) LSV curves of the first and 1000th repeated cycles at 10 mV s^{-1}.

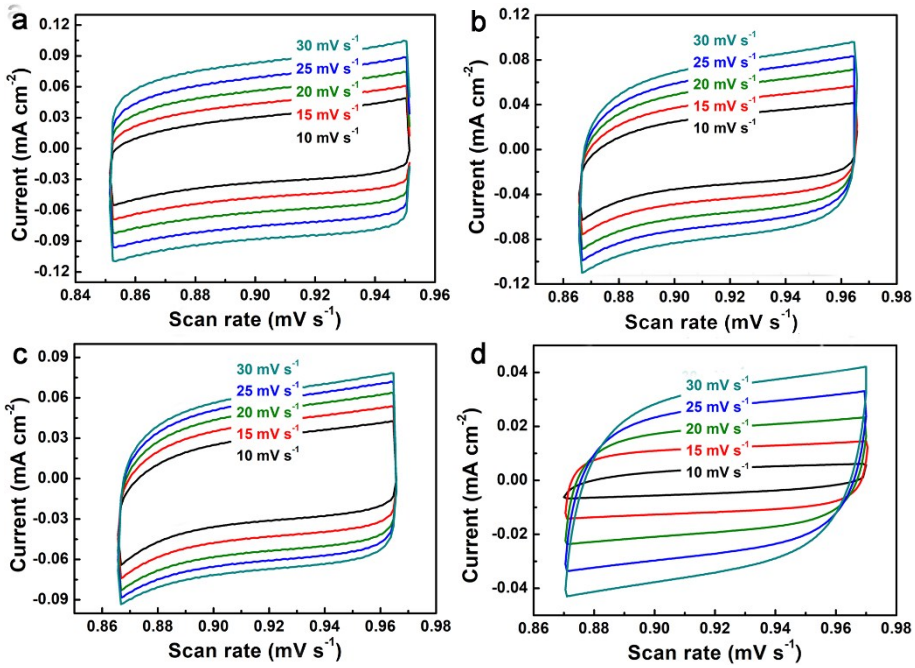

Fig. S20 CV curves of the 20 wt% Pt/C (a), Fe/Fe_3C@N-C (b), N-C (c), and Fe/Fe_3C (d) in non-Faraday regions at different scan rate in 1 M KOH solution.

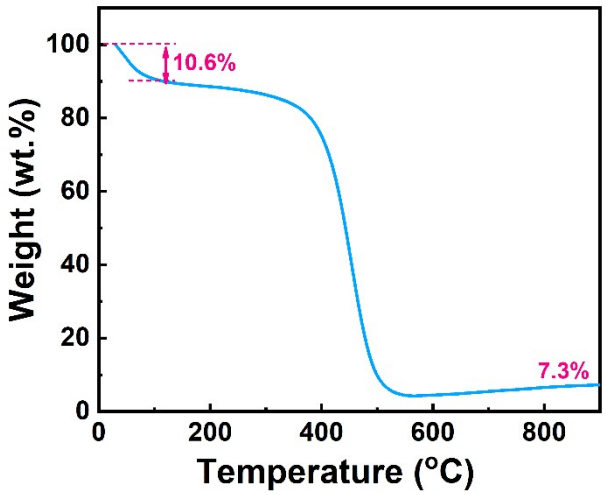

Fig. S21 TGA curve of Fe/Fe_3C@N-C (obtained at 600 °C) with a heating rate of 5 °C min^{-1} in air.

As shown in Figure S21, the weight loss (10.6 wt%) before 100 °C is attributed to the adsorbed water. Both the combustion of carbon and oxidation of Fe/Fe_3C species exist in the temperature range of 300~550 °C, leading to an obvious weight loss. Only oxidation of the remaining Fe/Fe_3C particles occurs at temperatures exceeding 550 °C, resulting a slight weight increase. The weight keeps almost constant when the temperature is higher than 800 °C, meaning that all carbon is depleted by combustion and all Fe/Fe_3C particles are converted to Fe_2O_3 by oxidation. Therefore, the 7.3 wt% mass in the final stage reflects the weight ratio of Fe_2O_3, which means that the mass ratio of Fe atom in Fe/Fe_3C@N-C is 5.7 wt%. The mass loading on the RDE electrode (5 mm in diameter) is 0.45 mg cm^{-2}, meaning that the number of Fe atom on the electrode is 9×10^{-8} mol. The N content is determined to be 0.8 wt% by XPS survey spectrum. Assuming that Fe/Fe_3C@N-C are consisted of C, N, and Fe elements, then the atomic ratio of Fe in Fe/Fe_3C@N-C is calculated to be 1.3 at% by the following equation:

$$Fe_{(at.\%)} = \frac{\frac{m_{Fe}}{M_{Fe}}}{\frac{m_{Fe}}{M_{Fe}}+\frac{m_N}{M_N}+\frac{m_C}{M_C}} = \frac{\frac{5.7}{56}}{\frac{5.7}{56}+\frac{0.8}{14}+\frac{93.5}{12}} = 1.3 \text{ at\%}$$

Considering the Fe atom is the center of active sites [11-13], then the Turnover Frequency

(TOF, the amount of H_2 per mol Fe per second) is calculated by the following equation:

$$TOF = \frac{j * A}{2 * F * m}$$

where j (A cm^{-2}) is the current density at a specific overpotential (here the selected overpotential is 300 mV), A is the electrode area of RDE (0.196 cm^2), 2 (mol) represents the electrons consumed for generating one mole of H_2, m is the number of Fe atoms (9×10^{-8} mol). F is the Faraday's constant (96485 C mol^{-1}).

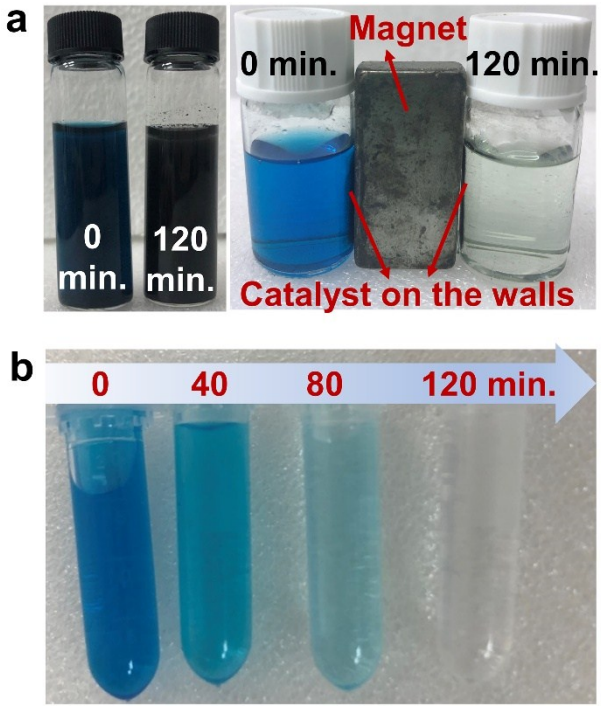

Fig. S22 (a) Optical images for the Fe/Fe_3C@N-C catalysts in the MB-containing solutions after degradation for 0 or 120 min. (The left two bottles: without a magnet; The right two bottles: with a magnet). (b) Optical images of the MB-containing solutions after degradation by Fe/Fe_3C@N-C for different times.

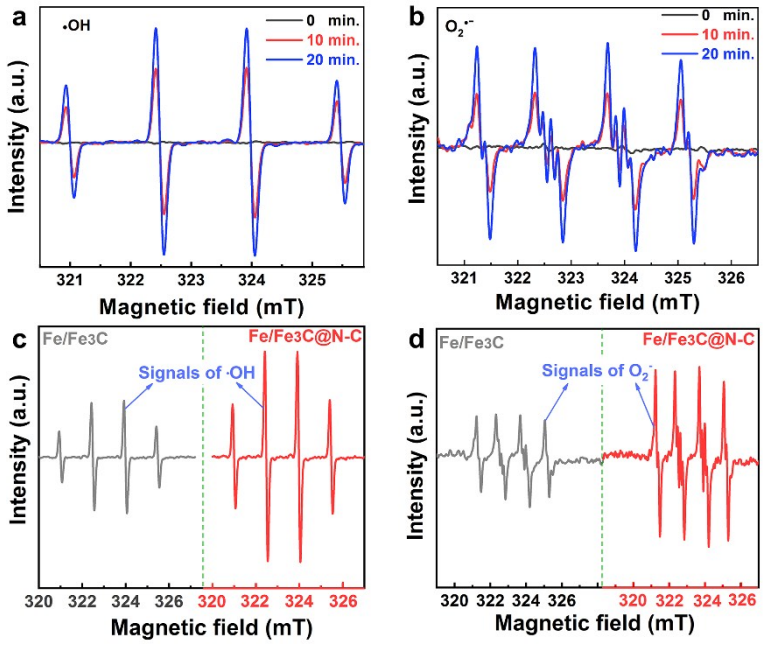

Fig. S23 The time-dependent variation of electronspin resonance (ESR) signals of (a) hydroxyl radical (·OH) and (b) superoxide ($O_2^{\cdot-}$) radical detected during degradation of MB by Fe/Fe_3C@N-C. Comparison of ·OH (c) and $O_2^{\cdot-}$ (d) signals detected by ESR during degradation of MB by Fe/Fe_3C and Fe/Fe_3C@N-C.

Table S1. Comparison of HER performances between recently reported literatures and this work

Catalysts	Electrolyte	$\eta_{@10\ mA\ cm^{-2}}$ (mV)	Tafel slope (mV dec^{-1})	j_0 (mA cm^{-2})	Refs.
Fe/Fe_3C@N-C	0.5 M H_2SO_4	147	78	0.3	This work
	1 M KOH	153	91	0.4	
Fe_3C-Co/N-C	0.5 M H_2SO_4	298	100.3	-	[4]
	1 M KOH	238	108.8	-	
$(Fe_{0.75}Co_{0.25})C_2$	1 M KOH	174	107	-	[5]
Fe-N-C	0.5 M H_2SO_4	130	89	0.027	[6]
Fe_3C encased in graphene nanoribbons	0.5 M H_2SO_4	49	46	-	[7]
$Co_2FeC_xN_y$	0.5 M H_2SO_4	180	90	-	[8]
Fe_xP in N-P codoped carbon	0.5 M H_2SO_4	227	81	0.023	[9]
FeCo in N-doped carbon nanotube	0.5 M H_2SO_4	284	72	-	[10]
FeCo in N-doped graphene	0.5 M H_2SO_4	262	74	-	[11]
Ni-doped FeP/carbon hollow nanorods	0.5 M H_2SO_4	72	54	0.723	[12]
	1 M KOH	95	72	-	
FeP/carbon hollow nanorods	0.5 M H_2SO_4	157	127	0.594	[12]
Mo_2C nanobelts	0.5 M H_2SO_4	140	51.3	0.021	[13]
	1 M KOH	110	49.7	0.056	
MoC-Mo_2C in porous N-doped carbon	1 M KOH	121	60	0.15	[14]
WC-W_2C in porous N-doped carbon	1 M KOH	101	90	0.74	[14]
N-doped Mo_2C	0.5 M H_2SO_4	177.5	59.6	0.010	[15]
S-vacancy MoS_2	0.5 M H_2SO_4	194	73	-	[16]

Supplementary References

1 C. Zeng, W. Weng, T. Lv and W. Xiao, *ACS Appl. Mater. Interfaces*, **2018**, 10, 30470-30478.

2 W. Weng, C. Zeng and W. Xiao, *ACS Appl. Mater. Interfaces*, **2019**, 11, 9156-9163.

3 X. Xin, H. Qin, H. P. Cong and S. H. Yu, *Langmuir*, **2018**, 34, 4952-4961.

4 C. C. Yang, S. F. Zai, Y. T. Zhou, L. Du and Q. Jiang, *Adv. Funct. Mater.*, **2019**, 29, 1901949.

5 S. Li, P. Ren, C. Yang, X. Liu, Z. Yin, W. Li, H. Yang, J. Li, X. Wang, Y. Wang, R. Cao, L. Lin, S. Yao, X. Wen and D. Ma, *Sci. Bull.*, **2018**, 63, 1358-1363.

6 X. Zeng, J. Shui, X. Liu, Q. Liu, Y. Li, J. Shang, L. Zheng and R. Yu, *Adv. Energy Mater.*, **2018**, 8, 1701345.

7 X. Fan, Z. Peng, R. Ye, H. Zhou and X. Guo, *ACS Nano*, **2015**, 9, 7407-7418.

8 P. Liu, Y. Liu, J. Jiang, S. Ashraf, X. Wu, G. Han, J. Gao, K. Zhang and B. Li, *ACS Sustai. Chem. Eng.*, **2019**, 7, 8744-8754.

9 Y. Cheng, J. Guo, Y. Huang, Z. Liao and Z. Xiang, *Nano Energy*, **2017**, 35, 115-120.

10 J. Deng, P. Ren, D. Deng, L. Yu, F. Yang and X. Bao, *Energy Environ. Sci.*, **2014**, 7, 1919-1923.

11 Y. Yang, Z. Lun, G. Xia, F. Zheng, M. He and Q. Chen, *Energy Environ. Sci.*, **2015**, 8, 3563-3571.

12 X. F. Lu, L. Yu and X. W. Lou, *Sci. Adv.*, **2019**, 5, eaav6009.

13 S. Jing, L. Zhang, L. Luo, J. Lu, S. Yin, P. K. Shen and P. Tsiakaras, *Appl. Catal. B-Environ.*, **2018**, 224, 533-540.

14 X. F. Lu, L. Yu, J. Zhang and X. W. D. Lou, *Adv. Mater.*, **2019**, 31, e1900699.

15 R. Jiang, J. Fan, L. Hu, Y. Dou, X. Mao and D. Wang, *Electrochim. Acta*, **2018**, 261, 578-587.

16 W. Wu, C. Niu, C. Wei, Y. Jia, C. Li and Q. Xu, *Angew. Chem. Int. Edit.*, **2019**, 58, 2029-2033.